MODELING AND ANALYSIS OF A BROADBAND PIEZOAEROELASTIC ENERGY HARVESTER

Vagner Candido de Sousa, vagner@sc.usp.br
Carlos De Marqui Júnior, demarqui@sc.usp.br
Department of Aeronautical Engineering, Engineering School of Sao Carlos - University of Sao Paulo, Av. Trabalhador Sancarlense 400, 13566-590, São Carlos, SP, Brazil

Abstract. *The conversion of flow-excited vibrations into electrical energy is a scalable option for energy harvesting. Stable aeroelastic LCO of acceptable amplitude can provide an important source of persistent electrical power. Therefore, a nonlinear aeroelastic system might be useful configuration for wind energy harvesting over a wide range of airflow speeds. In a previous work, the modeling and analysis of a piezoelectric energy harvester with two degrees of freedom (DOF), i.e. pitch and plunge, was presented. A combined nonlinearity (free play and cubic hardening) was modeled in the pitch DOF. Bounded flutter over a wide range of airflow speeds (ranging from velocities slightly below the linear flutter speed up to 1.5 of the linear flutter speed) was obtained, providing a useful piezoaeroelastic harvester. However, LCO below the linear flutter speed would be the most interesting case for practical applications (natural wind). In this paper, a piezoaeroelastically coupled lumped-parameter model for wind energy harvesting is presented. An airfoil with three DOF, i.e. pitch, plunge and control surface rotation, is investigated. Piezoelectric coupling is introduced to the plunge DOF and a resistive load is considered in the electrical domain of the problem. The unsteady aerodynamic loads are obtained from Jones' approximation of Wagner's indicial function. The piezoaeroelastic equations are cast in the state-space form. Two case studies are presented in this work for energy harvesting from aeroelastic oscillations. First the interaction between piezoelectric power generation and linear aeroelastic response of the typical section is investigated. Time domain predictions for pitch, control surface and plunge DOF as well as electrical power output are presented. In the second case, free play nonlinearity is modeled in the control surface DOF. The piezoaeroelastic behavior is investigated over a wide range of airflow speeds and a set of load resistances in the electrical domain (ranging from short-circuit to open-circuit condition). A useful configuration leading to oscillations over a wide range of airflow speeds (from 18% to 94% of the linear flutter speed) is presented.*

Keywords*: broadband harvester, energy harvesting, aeroelasticity, piezoelectricity*

1. INTRODUCTION

Scavenging vibration energy with piezoelectric materials is a novel solution for applications where traditional powering is prohibitive (expensive or impracticable). Anton and Sodano (2007) present a review of vibration power harvesting using piezoelectric materials. They recall that electrochemical batteries have limited life and thus periodic replacement must be performed. This is an issue for devices placed on remote locations as an arctic monitoring station (Pimentel, Musilek and Knight, 2010).

Cook-Chennault, Thambi and Sastry (2008) present an extensive discussion about non-regenerative and regenerative power supplies for microelectromechanical systems. They mention that regenerative technologies can be implemented for both standalone and hybrid power systems and include microphotovoltaic arrays, microthermophotovoltaic cells, electromagnetic and inductively coupled plasmas, acoustic noise, thermoelectric, electrostatic and piezoelectric devices. The authors also point out that vibration-based energy harvesting devices have power densities comparable to thin- and thick-film lithium and lithium-ion batteries. This fact explains the increasing attention that piezoelectric energy harvesters have received.

Recently the concept of self-charging structures (Anton, Erturk and Inman, 2010) has been introduced to improve multifunctionality in UAVs (unmanned air vehicles). The proposed multilayer structure is composed of piezoceramic layers for vibration-to-electric energy conversion, thin-film battery layers for storing the generated energy and a metallic substructure layer as the original load-bearing layer. An electromechanically coupled finite element (FE) model (De Marqui *et al*., 2009) has been successfully verified against the analytical results obtained from the closed-form solution for a unimorph harvester under base excitation (Erturk and Inman, 2008) and also against the analytical and experimental results for a bimorph energy harvester with a tip mass under base excitation (Erturk and Inman, 2009). The FE model has also been used to solve an optimization problem for UAV applications. The aluminum wing spar of a UAV is modified to design a generator wing spar. Since mass densities of typical piezoceramic materials are considerably large for UAV applications, a limiting value for mass addition is imposed to the problem as a design constraint. Dimensions of the embedded piezoceramic device are identified for the maximum electrical power output of the generator spar.

In the field of aeroelasticity, the possibility of an additional power source for UAV and micro air vehicles (MAV) is attractive. Usable power can be extracted from aeroelastic vibrations of lifting surfaces. De Marqui *et al*. (2011) present

a piezoaeroelastic frequency-domain analysis of a cantilevered plate-like wing for energy harvesting. The piezoaeroelastic equations are obtained by combining an electromechanical finite-element plate model with the doublet-lattice method. Expressions for piezoaeroelastically coupled frequency response functions are also defined.

Erturk *et al*. (2010) present a frequency domain analysis of a linear piezoaeroelastically coupled typical section. The harvester delivers 10.7 mW of power to a 100 $\mathrm{k}\Omega$ load resistance under a flow excitation of 9.3 m/s. Self-sustained oscillations occurring at a specific airspeed is a limiting situation for such a wind energy harvester. On the other hand, structural nonlinearities (Lee, Price and Wong, 1998) can induce subcritical limit cycle oscillations (LCO). Nonlinear LCO over a wide range of airflow speeds provides a useful source of electrical power. Recently, Anicézio *et al*. (2011) presented a theoretical model with experimental validation for a nonlinear piezoaeroelastic typical section. A free play region was modeled in the pitch DOF. LCO of acceptable amplitude was obtained below the linear flutter speed and the power output (about 30 mW) is twice the power of the linear model. The same paper suggests that a cubic stiffening nonlinearity bounds the amplitudes of LCO, improving the operating envelope of such an energy harvester. In addition to scavenging energy, Dunnmon *et al*. (2011) establish metrics regarding to the efficiency of a harvester. The authors define transduction efficiency as the ratio of the energy absorbed from the host structure by the electrical system.

In this paper a broadband configuration of energy harvester is presented. The model presented here is similar (electromechanical coupling is added) to the one by Tang, Dowell and Virgin (1998). Two case studies are presented. First the influence of the control surface stiffness is investigated in a linear case. Although the critical flutter speed reduced from 23.96 m/s to 3.50 m/s for specific control surface stiffness, self-sustained oscillations occurring at a specific airflow speed still restricts the envelope of such a harvester. Then a nonlinear case study is presented. Free play is modeled in the control surface DOF and the operating envelope ranges from 18% to 94% of the critical condition (linear flutter velocity).

2. PIEZOAEROELASTIC MODEL

Figure 1 shows the schematic of a 3-DOF aeroelastic typical section. The plunge, pitch and control surface displacement variables are denoted by h, α and β, respectively. The plunge displacement is measured at the elastic axis (positive in the downward direction) and the pitch angle is measured at the elastic axis (positive in the clockwise direction). The control surface angle is measured from the typical section chord line (positive in the clockwise direction). In addition, b is the semichord of the airfoil section, e is the nondimensional distance of elastic axis from the mid-chord position, c is the nondimensional distance of the control surface hinge line from the mid-chord, x_α is the dimensionless chord-wise offset of the elastic axis from the centroid (CG), x_β is the dimensionless offset of the control surface CG from the hinge line, k_h is the stiffness per length in the plunge DOF, k_α is the stiffness per length in the pitch DOF, k_β is the stiffness per length in the control surface DOF, b_h is the damping coefficient per length in the plunge DOF, b_α is the damping coefficient per length in the pitch DOF, b_β is the damping coefficient per length in the control surface DOF and U is the airflow speed.

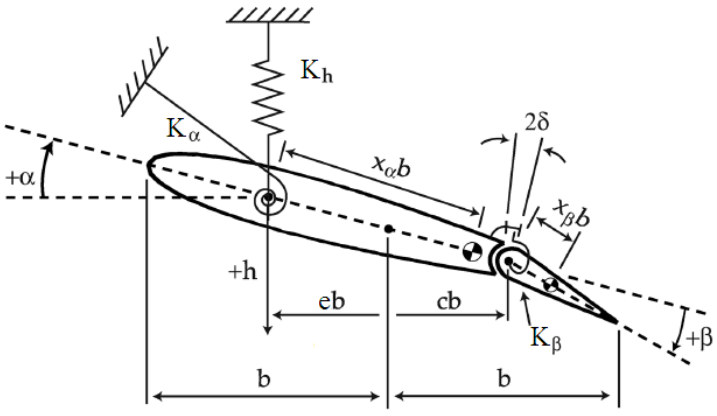

Figure 1. 3-DOF typical aeroelastic section with control surface (adapted from Tang and Dowell, 2010)

In this work, piezoelectric coupling is added to the plunge DOF of the typical section. A load resistance is considered in the electrical domain of the problem. A concentrated nonlinearity (free play) is added to the control surface DOF. Therefore, by using Lagrange's equations, the nonlinear piezoaeroelastically coupled equations are presented as

$$(m+m_e)\ddot{h}+S_\alpha\ddot{\alpha}+S_\beta\ddot{\beta}+b_h\dot{h}+k_h h-\theta v_p/l=-L \tag{1.a}$$

$$I_\alpha\ddot{\alpha}+(I_\beta+b(c-a)S_\beta)\ddot{\beta}+S_\alpha\ddot{h}+b_\alpha\dot{\alpha}+k_\alpha\alpha=M_\alpha \tag{1.b}$$

$$(I_\beta+b(c-a)S_\beta)\ddot{\alpha}+I_\beta\ddot{\beta}+S_\beta\ddot{h}+b_\beta\dot{\beta}+k_\beta\beta+f_{fp}(\beta)=M_\beta \tag{1.c}$$

$$C_p^{eq}\dot{v}_p+\frac{v_p}{R_l}+\theta\dot{h}=0 \tag{1.d}$$

where m is the airfoil mass per length (in the span direction), m_e is the fixture mass (connecting the airfoil to the plunge springs) per length, I_α is the airfoil mass moment of inertia per length about the elastic axis and I_β is the control surface moment of inertia per length about its hinge line, S_α and S_β are the static moments per length, l is the span length, R_l is the load resistance in the electrical domain, v_p is the voltage across the resistive load, C_p^{eq} is the equivalent capacitance of the piezoceramic layers, θ is the electromechanical coupling term, M_α and M_β are the aerodynamic moments, L is the aerodynamic lift and the over-dot represents differentiation with respect to time. In Eq. (1c), $f_{fp}(\beta)$ is given by

$$f_{fp}(\beta)=\begin{cases}-k_\beta\beta_{fp}, & \beta>\beta_{fp}\\ 0, & -\beta_{fp}\le\beta\le\beta_{fp}\\ k_\beta\beta_{fp}, & \beta<-\beta_{fp}\end{cases} \tag{2}$$

and β_{fp} is the free play gap. It is important to note that when $\beta_{fp}\neq 0$ the free play nonlinearity is obtained (combining the linear restoring moment and $f_{fp}(\beta)$). The linear equations are obtained when $\beta_{fp}=0$. The restoring moment in the control surface DOF for the free play nonlinearity is presented in Fig. 2 along with the linear case.

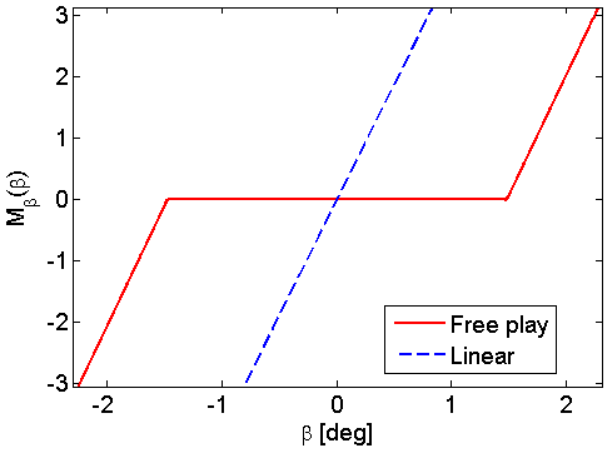

Figure 2. Linear and nonlinear elastic restoring moments of the control surface

The normalized version of the piezoaeroelastic equations is obtained by multiplying equation (1a) by $1/(mb)$ and (1b) and (1c) by $1/(mb^2)$. The electric equation is also multiplied by $1/(mb^2)$. The piezoaeroelastic equations are presented as,

$$\mu\ddot{\bar{h}}+x_\alpha\ddot{\alpha}+x_\beta\ddot{\beta}+\zeta_h\dot{\bar{h}}+\omega_h^2\bar{h}-\bar{\theta}v_p/l=-\bar{L} \tag{3.a}$$

$$r_\alpha^2\ddot{\alpha}+(r_\beta^2+(c-a)x_\beta)\ddot{\beta}+x_\alpha\ddot{\bar{h}}+\zeta_\alpha\dot{\alpha}+r_\alpha^2\omega_\alpha^2\alpha=\bar{M}_\alpha \tag{3.b}$$

$$(r_\beta^2 + (c-a)x_\beta)\ddot{\alpha} + r_\beta^2\ddot{\beta} + x_\beta\ddot{\bar{h}} + \zeta_\beta\dot{\beta} + r_\beta^2\omega_\beta^2\beta + \bar{f}_{fp}(\beta) = \bar{M}_\beta \tag{3.c}$$

$$\bar{C}_p^{eq}\dot{\bar{v}}_p + \frac{\bar{v}_p}{\bar{R}_l} + \bar{\theta}^*\dot{\bar{h}} = 0 \tag{3.d}$$

where $\mu = (m+m_e)/m$, ζ_h, ζ_α and ζ_β are the plunge, pitch and control surface damping ratios, respectively (subscript h refers to plunge, subscript α refers to pitch and subscript β refers to the control surface), ω_h, ω_α and ω_β are the uncoupled natural frequencies, r_α and r_β are the dimensionless radius of gyration, $\bar{h} = h/b$, $\bar{v}_p = v_p/v^*$ (where v^* = 1 Volt), $\bar{L}$, $\bar{M}_\alpha$ and $\bar{M}_\beta$ are the dimensionless aerodynamic loads, $\bar{\theta} = (\theta v^*/mbl)$, $\bar{C}_p^{eq} = (C_p^{eq}v^*/mb^2l)$, $\bar{R}_l = (R_l mb^2 l/v^{*2})$ and $\bar{\theta}^* = (\theta v^*/mb^2 l)$, or $\bar{\theta}^* = \bar{\theta}/b$. The term $\bar{f}_{fp}(\beta)$ is the modified version of Eq. (2).

The linear piezoaeroelastic equations (Eq. (3a-d)) is represented here in the state-space form proposed by Edwards, Ashley and Breakwell (1979). However, the electromechanical coupling is also included in this paper. Therefore an additional electrical state is considered here. The unsteady aerodynamic loads (lift and moments in Eq.(3)) due to arbitrary motions are obtained from Jones' approximation of Wagner's indicial function, which is an approximation to the generalized Theodorsen function. The load expressions for arbitrary values of s (Laplace variable) are obtained from the representation of simple harmonic loads by a rational function of s. The rational function describing the aerodynamic loads is ordinary differential equations that can be cast into state space form. Therefore two augmented states ($\mathbf{x}_a = \{x_1 \quad x_2\}^T$) are included in the state space representation of the piezoaeroelastic problem (T denotes transposed). The linear state-space piezoaeroelastic equation is

$$\begin{bmatrix} \mathbf{I} & \mathbf{0} & \mathbf{0} & \mathbf{0} \\ \mathbf{0} & \tilde{\mathbf{M}} & \mathbf{0} & \mathbf{0} \\ \mathbf{0} & \mathbf{0} & \mathbf{I} & \mathbf{0} \\ \mathbf{0} & \mathbf{0} & \mathbf{0} & \bar{C}_p^{eq} \end{bmatrix} \begin{Bmatrix} \dot{\mathbf{x}} \\ \ddot{\mathbf{x}} \\ \dot{\mathbf{x}}_a \\ \dot{\bar{v}}_p \end{Bmatrix} = \begin{bmatrix} \mathbf{0} & \mathbf{I} & \mathbf{0} & \mathbf{0} \\ -\tilde{\mathbf{K}} & -\tilde{\mathbf{B}} & \mathbf{D} & \mathbf{\Theta}_s \\ \mathbf{E}_1 & \mathbf{E}_2 & \mathbf{F} & \mathbf{0} \\ \mathbf{0} & \mathbf{\Theta}_e & \mathbf{0} & 1/\bar{R}_l \end{bmatrix} \begin{Bmatrix} \mathbf{x} \\ \dot{\mathbf{x}} \\ \mathbf{x}_a \\ \bar{v}_p \end{Bmatrix} \tag{4}$$

where $\mathbf{\Theta}_s = [0 \quad 0 \quad \bar{\theta}]^T$, $\mathbf{\Theta}_e = [0 \quad 0 \quad -\bar{\theta}^*]^T$, $\mathbf{x} = \{\alpha \quad \beta \quad \bar{h}\}^T$ and $\mathbf{I}$ is the identity matrix. The mass, stiffness and damping related matrices in Eq. (4) are

$$\tilde{\mathbf{M}} = \mathbf{M} - \frac{\rho b^2}{m}\mathbf{M}_{nc}$$

$$\tilde{\mathbf{K}} = \mathbf{K} - \frac{\rho b^2}{m}(\tfrac{U}{b})^2(\mathbf{K}_{nc} + 0.5\mathbf{R}\mathbf{S}_1)$$

$$\tilde{\mathbf{B}} = \mathbf{B} - \frac{\rho b^2}{m}(\tfrac{U}{b})(\mathbf{B}_{nc} + 0.5\mathbf{R}\mathbf{S}_2)$$

where $\mathbf{M}$ is the structural mass matrix, $\mathbf{B}$ is the structural damping matrix, $\mathbf{K}$ is the structural stiffness matrix, ρ is the air density and $\mathbf{M}_{nc}$, $\mathbf{B}_{nc}$ and $\mathbf{K}_{nc}$ are noncirculatory aerodynamic matrices related to inertia, damping and stiffness. These matrices together with the aerodynamic matrices $\mathbf{D}$, $\mathbf{E}_1$, $\mathbf{E}_2$, $\mathbf{F}$, $\mathbf{R}$, $\mathbf{S}_1$ and $\mathbf{S}_2$ are given in Edwards, Ashley and Breakwell (1979).

Equation (4) can be also represented as

$$\dot{\tilde{\mathbf{x}}} = \mathbf{A}\tilde{\mathbf{x}} \tag{5}$$

and

$$\mathbf{A} = \begin{bmatrix} \mathbf{0} & \mathbf{I} & \mathbf{0} & \mathbf{0} \\ -\tilde{\mathbf{M}}^{-1}\tilde{\mathbf{K}} & -\tilde{\mathbf{M}}^{-1}\tilde{\mathbf{B}} & \tilde{\mathbf{M}}^{-1}\mathbf{D} & \tilde{\mathbf{M}}^{-1}\boldsymbol{\Theta}_s \\ \mathbf{E}_1 & \mathbf{E}_2 & \mathbf{F} & \mathbf{0} \\ \mathbf{0} & 1/\bar{C}_p^{eq}\ \boldsymbol{\Theta}_e & \mathbf{0} & 1/\bar{C}_p^{eq}\ (1/\bar{R}_l) \end{bmatrix}$$

$$\tilde{\mathbf{x}} = \{\mathbf{x} \quad \dot{\mathbf{x}} \quad \mathbf{x}_a\}^T$$

A similar derivation is performed when concentrated nonlinearities (Eq. (2)) are included in the piezoaeroelastic system (Eq. (1)). In such a case, a combination of linear state-space models is used to represent the full nonlinear system (Conner, Virgin and Dowell, 1996). Therefore, the nonlinear state-space equation is

$$\dot{\tilde{\mathbf{x}}} = \mathbf{A}_i\tilde{\mathbf{x}} + \mathbf{a}_i \tag{6}$$

where the state matrix and the vector $\mathbf{a}_i$ changes as the system reaches the free play boundaries (Fig. 2). The equations are solved using a Runge-Kutta algorithm with Hénon's method (Hénon, 1982). Conner, Virgin and Dowell (1996) presented the adaptation of Hénon's method to determine the switching point (or free play boundaries) in the time domain and avoid errors in numerical integration and numerical instability.

3. CASE STUDIES

Two study cases are presented in this work. In the first case, a linear piezoaeroelastic problem is investigated. The linear flutter speed is determined for a set of resistors ranging from close to short-circuit to close to open-circuit boundary conditions ($R_l = 10^2$, 10^3, 10^4, 10^5 and $10^6\ \Omega$). The optimum load resistance that gives the maximum power and maximum flutter speed (due to shunt damping effect of resistive power generation) is determined. The flutter boundary is also investigated for different control surface uncoupled natural frequency to the pitch uncoupled natural frequency ratios. In the second case, a nonlinear system is considered. The linear torsional spring of the control surface DOF is replaced by a bilinear spring with a free play region. The system parameters used in this paper are presented in Tab. 1 and are the same given by Tang, Dowell and Virgin (1998). The electromechanical coupling term θ = 1.55 mN/V was obtained from a distributed parameter model (Erturk and Inman, 2008). The piezoelectric manufacturer's published equivalent capacitance C_p^{eq} = 120 nF.

Table 1. System parameters (Tang, Dowell and Virgin, 1998).

Semichord	0.127 m
Span	0.52 m
Elastic axis	-0.5
Hinge line	0.5
Airfoil-control surface mass (per span)	1.558 Kg/m
Fixture mass (per span)	0.913 x 2 Kg/m
S_α (per span)	0.08587 Kg
S_β (per span)	0.00395 Kg
x_α	0.434
x_β	0.01996
I_α (per span)	0.01347 Kgm
I_β (per span)	0.0003264 Kgm
k_α (per span)	37.3 Kgm/s^2
k_β (per span)	3.9 Kgm/s^2
k_h (per span)	2818.8 Kg/m/s^2
ζ_α	0.01626
ζ_β	0.0115
ζ_h	0.0113

3.1. Linear Piezoaeroelastic Model

The piezoaeroelastic behavior of the electromechanically coupled linear typical section is investigated. The frequency ratio $\omega_\beta / \omega_\alpha$ is 2.1 (corresponding to the nominal stiffness $k_\beta = 3.9$ Kgm/s^2).

The stability of this system is investigated through the analysis of the real part of eigenvalues. The short-circuit flutter speed is $U = 23.96$ m/s (for $R_l = 10^2\,\Omega$). The optimum load resistance $R_l = 10^5\,\Omega$ gives the linear flutter speed of $U = 24.02$ m/s. The maximum power given by the optimum load is 4.6 mW. The variation of power output against the load resistance is shown in Fig. 3.

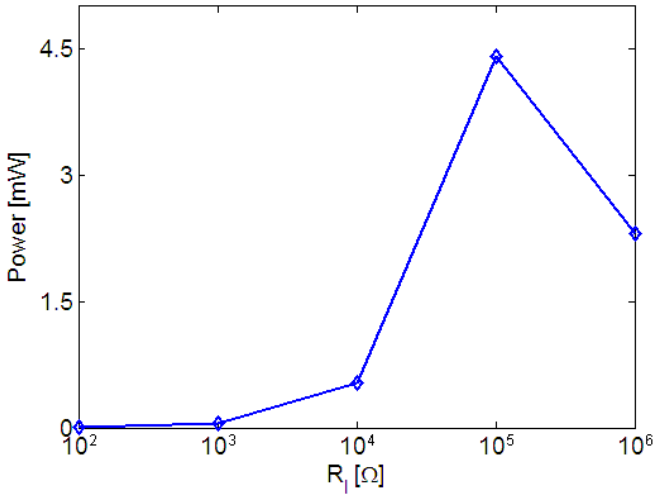

Figure 3. Predicted power output for each load resistance

The influence of the control surface uncoupled frequency to the pitch uncoupled frequency ratio ($\omega_\beta / \omega_\alpha$) over the linear flutter boundary is shown in Fig. 4 (short-circuit condition).

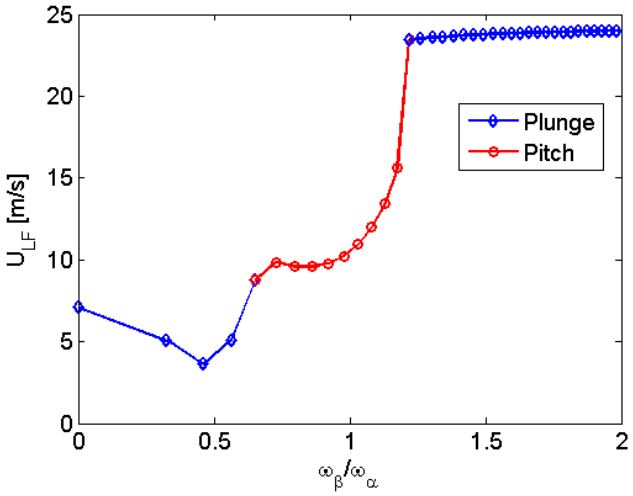

Figure 4. Linear flutter velocity for different frequency ratios (◊ = plunge, ○ = pitch)

When the control surface stiffness is zero ($\omega_\beta / \omega_\alpha = 0$) the short-circuit flutter speed is 7.04 m/s. For the optimal load resistance and control surface free condition, the linear flutter speed is 7.10 m/s (and the power obtained is 3.4 mW).

When $\omega_\beta / \omega_\alpha = 0.48$, corresponding to $k_\beta = 0.21$ Kgm/s^2, the linear short-circuit flutter speed is $U = 3.50$ m/s. This is the lowest airflow speed for which persistent oscillations may occur for the linear case. When the optimal load is considered for this frequency ratio the linear flutter speed is 3.6 m/s.

Figure 5 shows the variation of power output (delivered at the flutter speed previously determined for each control surface stiffness considered in this work) against the variation of control surface stiffness (for $R_l = 100$ kΩ). The maximum power is obtained for $\omega_\beta / \omega_\alpha$ larger than 1.2 (that gives large plunge displacements). However the linear flutter speed is not practical for this range of frequency ratios (Fig. 4). When the frequency ratio is $0.75 < \omega_\beta / \omega_\alpha < 1.2$ plunge displacement is small as well as power output.

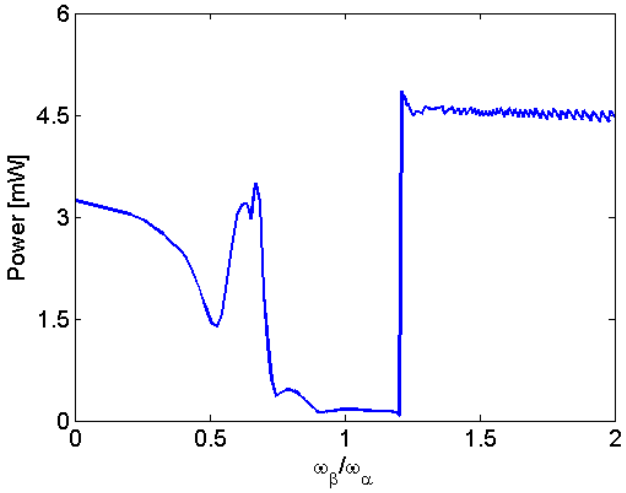

Figure 5. Electrical power output for different frequency ratios

3.2. Nonlinear Piezoaeroelastic Model

In the second case study, a concentrated nonlinearity is modeled in the control surface DOF. The linear torsional spring of the control surface DOF is replaced by a bilinear spring. The free play nominal gap is $2\delta = 4.24$ degrees and is symmetrical about the control surface zero position. For this configuration a limit cycle occurs at $U = 4.33$ m/s for a sufficiently large initial disturbance (and short-circuit condition). Such a minimum initial disturbance is shown to be $h/(\delta b) \sim 0.3$ (δ in radians) or about 1% of the semichord length (Tang, Dowell and Virgin, 1998). The authors also pointed out that the disturbance required to excite the plunge mode is smaller than that for the pitch and control surface DOFs.

The airflow velocity at which the first limit cycle occurs is 18% smaller than the linear flutter speed. Figure 6 (a-c) shows the nondimensional pitch, control surface and plunge amplitudes of LCO against the nondimensional flow velocity $\bar{u} = U / U_{F0}$ for the frequency ratio $\omega_\beta / \omega_\alpha = 2.1$ (where U_{F0} is the flutter airspeed for $\omega_\beta / \omega_\alpha = 0$ of the linear case). The nondimensional amplitudes of LCO are obtained by dividing the dimensional amplitudes by $2\pi\delta b / 180$. Figure 6 (d) shows the corresponding electrical power output for each load resistance considered in this work.

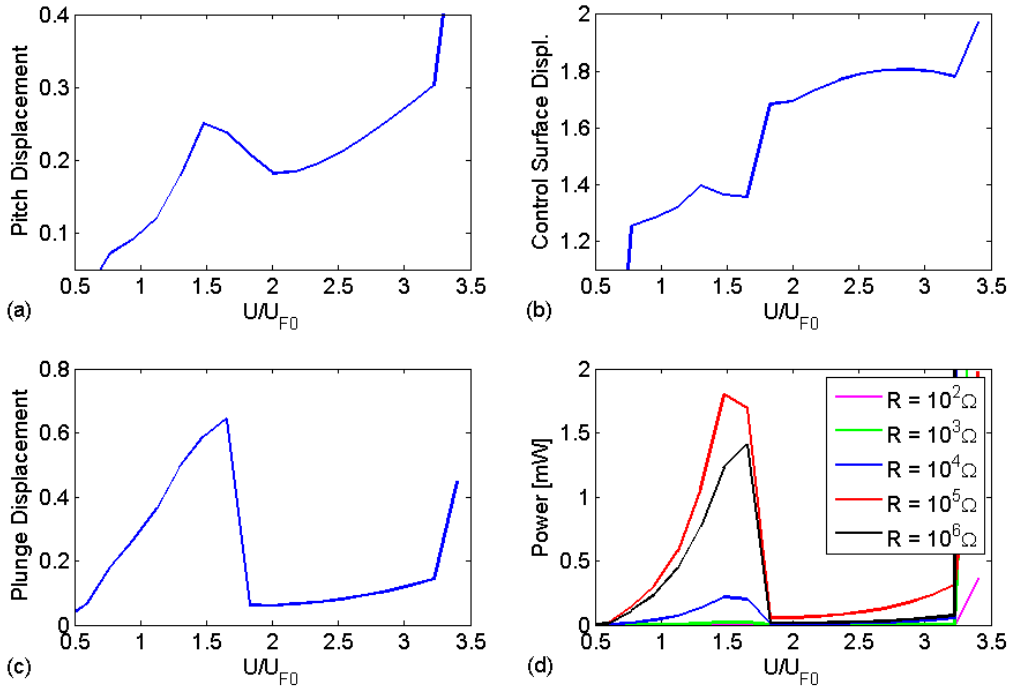

Figure 6. Nonlinear piezoaeroelastic responses with nondimensional velocity: (a-c) Nondimensional pitch, control surface and plunge amplitudes of LCO; (d) Electrical power output for each load resistance

One can note in Fig. 6 that any initial disturbance is damped out for any $\bar{u}$ lower than 0.6 and no persistent power output is obtained. For any velocity ratio larger than 0.6 the system undergoes self-sustained oscillations (for a finite initial disturbance).

For velocity ratios ranging from 0.6 to 1.7 there is a stable low-frequency limit cycle. The plunge amplitude of LCO grows with increasing airflow velocity and power increases from 70 μW up to 1.9 mW.

At $\bar{u} \sim 1.7$ the low-frequency LCO becomes unstable and a high-frequency LCO occurs. Such a change in the system response is followed by a sudden drop in the plunge amplitude. Between $1.8 < \bar{u} < 3.2$, the plunge displacement is bounded and exhibits a quite small increase with a relative large increase in the flow velocity. In this region, the power obtained for the optimal load increases from 55 μW to 300 μW.

For $\bar{u} > 3.2$ the frequency of oscillation tends to approach the plunge natural frequency and the amplitude of LCO (for the plunge, pitch and control surface DOF) grows up rapidly as the airflow approaches the linear flutter speed. Divergent motion will occur at 94% of the linear flutter speed.

The load resistance $R_l = 100\ \text{k}\Omega$ provides the maximum power among the loads considered in this paper. When $0.6 < \bar{u} < 1.7$ the most interesting situation for wind energy harvesting is verified. The airflow ranges from 18% up to 48% of the linear flutter speed and matches natural wind. The limit cycles are stable and the plunge amplitude increases with increasing airflow speed. Power increases from 70 μW to 1.9 mW (an increase of 27 times). Between $1.8 < \bar{u} < 3.2$ the power obtained ranges from 55 μW up to 300 μW.

4. CONCLUSIONS

This paper investigates theoretically and experimentally a linear and a nonlinear 3DOF piezoaeroelastic energy harvester. The piezoelectric coupling is introduced through the plunge DOF while the concentrated structural nonlinearity is introduced to the control surface DOF. A state-space piezoaeroelastic model is derived and the unsteady aerodynamic loads are obtained from Jones' approximation of Wagner's indicial function, which is an approximation to the generalized Theodorsen function. The linear piezoaeroelastic behavior is investigated for a set of load resistances. The optimum load that gives the maximum power also presents the largest flutter speed. The influence of control surface stiffness over the flutter speed is also investigated. A specific stiffness (or control surface to pitch frequency ratio) presents the minimum flutter speed (3.5 m/s), an interesting condition for energy harvesting from natural wind. Although usually avoided in real aircraft, the flutter condition is the ideal scenario for energy harvesting from linear aeroelastic vibrations.

The nonlinear piezoaeroelastic behavior of the electromechanically coupled typical section is also investigated. Free play nonlinearity is considered in the control surface DOF to reduce the cut-in speed of persistent oscillations. For this configuration a limit cycle is observed at U = 4.33 m/s for a sufficiently large initial disturbance (and short-circuit condition). The piezoaeroelastic behavior is investigated for a wide range of airflow speeds and persistent oscillations are obtained. The maximum power output of the configuration with free play nonlinearity is observed to be half of that of the linear configuration (at the flutter boundary). However, it is important to note that power can be extracted over a wide range of flow speeds in the nonlinear case. This is an interesting condition for practical applications.

5. ACKNOWLEDGMENTS

The authors gratefully acknowledge CNPq and FAPEMIG for partially funding the present research work through the INCT-EIE. The authors also gratefully acknowledge the support of CNPq (558646/2010-7 and 484132/2010-5).

6. REFERENCES

Anicézio, M.M., De Marqui Jr., C., Erturk, A. and Inman, D.J., 2011, "Nonlinear modeling and analysis of a piezoaeroelastic energy harvester", Proceedings of the XIV International Symposium on Dynamic Problems of Mechanics (DINAME 2011), ABCM, São Sebastião, SP , Brazil.

Anton, S.R. and Sodano, H.A., 2007, "A review of power harvesting using piezoelectric materials (2003-2006)", Smart Materials and Structures, Vol. 16, pp. R1-R21, doi:10.1088/0964-1726/16/3/R01.

Anton, S.R., Erturk, A. and Inman, D.J., 2010, "Multifunctional self-charging structures using piezoceramics and thin-film batteries", Smart Materials and Structures, Vol. 19., pp. 15, doi:10.1088/0964-1726/19/11/115021.

Conner, M.D., Virgin, L.N. and Dowell, E.H., 1996, "Accurate numerical integration of state space models for aeroelastic systems with free play", AIAA Journal, Vol. 34, No. 10, pp. 2202-2205.

Cook-Chennault, K.A., Thambi, N. and Sastry, A.M., 2008, "Powering MEMS portable devices - a review of non-regenerative and regenerative power supply systems with special emphasis on piezoelectric energy harvesting systems", Smart Materials and Structures, Vol. 17, pp. 30.

De Marqui Jr., C., Erturk, A. and Inman, D.J., 2009, "An electromechanical finite element model for piezoelectric energy harvester plates", Journal of Sound and Vibration, Vol. 327, pp. 9-25.

De Marqui Jr., C., Vieira, W.G.R., Erturk, A. and Inman, D.J., 2011, "Modeling and analysis of piezoelectric energy harvesting from aeroelastic vibrations using the doublet-lattice method", Journal of Vibration and Acoustics, Vol. 133, pp. 011003.

Dunnmon, J.A., Stanton, S.C., Mann, B.P. and Dowell, E.H., 2011, "Power extraction from aeroelastic limit cycle oscillations", Journal of Fluids and Structures, doi:10.1016/j.jfluidstructs.2011.02.003.

Edwards, J.W., Ashley, H. and Breakwell, J.V., 1979, "Unsteady aerodynamic modeling for arbitrary motions", AIAA Journal, Vol. 17, No. 4, pp. 365-374.

Erturk, A. and Inman, D.J., 2008, "A distributed parameter electromechanical model for cantilevered piezoelectric energy harvesters", ASME Journal of Vibration and Acoustics, Vol. 130, pp. 041002.

Erturk, A. and Inman, D.J., 2009, "An experimentally validated bimorph cantilever model for piezoelectric energy harvesting from base excitations", Smart Materials and Structures, Vol. 18, pp. 025009.

Erturk, A., Vieira, W.G.R., De Marqui Jr., C. and Inman, D.J., 2010, "On the energy harvesting potential of piezoaeroelastic systems," Applied Physics Letters, Vol. 96, pp. 184103.

Hénon, M., 1982, "On the numerical computation of Poincaré maps". Physica 5D, pp. 412-414.

Lee, B.H.L., Price, S.J. and Wong, Y.S., 1999, "Nonlinear aeroelastic analysis of airfoils: bifurcation and chaos", Progress in Aerospace Sciences 35, pp. 205-334.

Pimentel, D., Musilek, P. and Knight, A., 2010, "Energy harvesting simulation for automatic arctic monitoring stations", IEEE Electrical Power & Energy Conference.

Tang, D., Dowell, E.H. and Virgin, L.N., 1998, "Limit cycle behavior of an airfoil with a control surface", Journal of Fluids and Structures, Vol. 12, pp. 839-858.

Tang, D. and Dowell, E.H., 2010, "Aeroelastic airfoil with free play at angle of attack with gust excitation", AIAA Journal, Vol. 48, No. 2, pp. 427-442.

5. RESPONSIBILITY NOTICE

The authors are the only responsible for the printed material included in this paper.